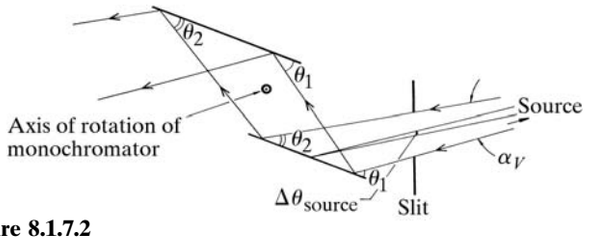

Figure 8.1.7.2
Double-crystal monochromator illuminated by SR. The contributions of the source divergence, α_V [less than or equal to γ^{-1}, equation (8.1.2.4), depending on the monochromator vertical entrance slit aperture; see also Colapietro *et al.* (1992)], and angular source size, $\Delta\theta_{\text{source}}$, to the range of energies reflected by the monochromator are shown. From Helliwell (1984). Reproduced with the permission of the Institute of Physics.

exit window of a high-pressure cell for protein-crystal high-pressure biophysical studies (Fourme *et al.*, 2001; Girard *et al.*, 2007). Such developments interact closely with machine and beamline specifications.

8.1.7.2.4. Crystal sample rocking width

The rocking width of a reflection depends on the horizontal and vertical beam divergence or convergence (after due account for collimation is taken), γ_H and γ_V, the spectral spreads $(\delta\lambda/\lambda)_{\text{conv}}$ and $(\delta\lambda/\lambda)_{\text{corr}}$, and the mosaic spread, η. We assume that the mosaic spread η is $\gg \omega$, the angular broadening of a reciprocal-lattice point (relp) due to a finite sample. In the case of synchrotron radiation, γ_H and γ_V are usually widely asymmetric. On a conventional source, usually $\gamma_H \simeq \gamma_V$. Two types of spectral spread occur with synchrotron (and neutron) sources. The term $(\delta\lambda/\lambda)_{\text{conv}}$ is the spread that is passed down each incident ray in a divergent or convergent incident beam; the subscript refers to the conventional source type. This is because it is similar to the $K\alpha_1, K\alpha_2$ line widths and separation. At the synchrotron, this component also exists and arises from the monochromator rocking width and finite-source-size effects. The term $(\delta\lambda/\lambda)_{\text{corr}}$ is special to the synchrotron or neutron case. The subscript 'corr' refers to the fact that the ray direction can be correlated with the photon or neutron wavelength. In this most general case, and for one example of a $(\delta\lambda/\lambda)_{\text{corr}}$ arising from the horizontal ray direction correlation with photon energy and the case of a horizontal rotation axis, the rocking width φ_R of an individual reflection is given by

$$\varphi_R = \left\{L^2\left[(\delta\lambda/\lambda)_{\text{corr}} d^{*2} + \zeta\gamma_H\right]^2 + \gamma_V^2\right\}^{1/2} + 2\varepsilon_s L, \qquad (8.1.7.8)$$

where

$$\varepsilon_s = (d^* \cos\theta/2)\left[\eta + (\delta\lambda/\lambda)_{\text{conv}} \tan\theta\right] \qquad (8.1.7.9)$$

and L is the Lorentz factor, $1/\left(\sin^2 2\theta - \zeta^2\right)^{1/2}$.

The Guinier setting of an instrument (curved crystal monochromator case, Fig. 8.1.7.1*b*) gives $(\delta\lambda/\lambda)_{\text{corr}} = 0$. The equation for φ_R then reduces to

$$\varphi_R = L\left[\left(\zeta^2\gamma_H^2 + \gamma_V^2/L^2\right)^{1/2} 2\varepsilon_s\right] \qquad (8.1.7.10)$$

(from Greenhough & Helliwell, 1982). For example, for $\zeta = 0$, $\gamma_V = 0.2$ mrad (0.01°), $\theta = 15°$, $(\delta\lambda/\lambda)_{\text{conv}} = 1 \times 10^{-3}$ and $\eta = 0.8$ mrad (0.05°), then $\varphi_R = 0.08°$. But φ_R increases as ζ increases [see Greenhough & Helliwell (1982), Table 5]. In the rotation/oscillation method as applied to protein and virus crystals, a small angular range is used per exposure. For example, the maximum rotation range per image, $\Delta\varphi_{\text{max}}$, may be 1.5° for a protein and

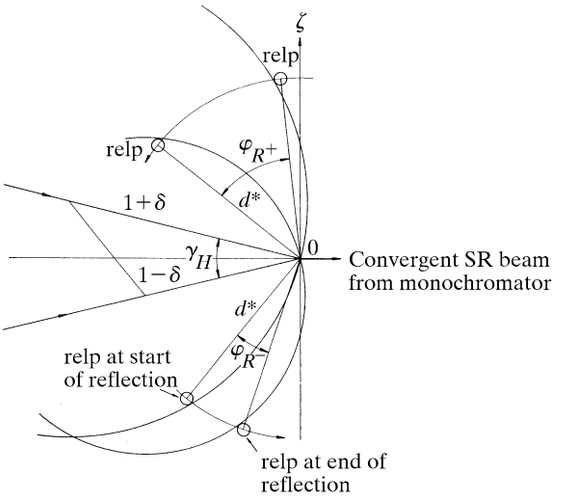

Figure 8.1.7.3
The rocking width of an individual reflection for the case of Fig. 8.1.7.1(*c*) and a vertical rotation axis. From Greenhough & Helliwell (1982).

0.4° or so for a virus. Many reflections will be only partially stimulated over the exposure. It is important, especially in the virus case, to predict the degree of penetration of the relp through the Ewald sphere. This is done by analysing the interaction of a spherical volume for a given relp with the Ewald sphere. The radius of this volume is given by

$$E \simeq \varphi_R/2L \qquad (8.1.7.11)$$

(Greenhough & Helliwell, 1982).

In Fig. 8.1.7.3, the relevant parameters are shown. The diagram shows $(\delta\lambda/\lambda)_{\text{corr}} = 2\delta$ in a plane, usually horizontal with a perpendicular (vertical) rotation axis, whereas the formula for φ_R above is for a horizontal axis. This is purely for didactic reasons since the interrelationship of the components is then much clearer.

The limits of protein-crystal rocking widths have been explored by Helliwell (1988), Colapietro *et al.* (1992) and Snell (1995), whereby arc-second crystal precision has been observed at room temperature, *i.e.* unfrozen protein crystals. Special analysis software (Lovelace *et al.*, 2000) has been written to extract such precise crystal mosaicity values and the experiment obviously requires stringent (usually undulator) collimation. Exact comparisons of mosaicity values need reflection indexing, *e.g.* see Snell *et al.* (1995).

8.1.8. Scientific utilization of SR in protein crystallography

There are a myriad of applications and results of the use of SR in crystallography. Helliwell (1992) gave an extensive survey and tabulations of SR and macromolecular crystallography applications; Chapter 9 therein concentrates on anomalous scattering and Chapter 10 on high resolution, large unit cells, small crystals, weak scattering efficiency and time-resolved data collection. The field has expanded so dramatically, in fact, that an equivalent survey today would be vast. Table 8.1.4.1 lists the web pages of the facilities, where the specifications and details of the beamlines can be found (*e.g.* all the publications at Daresbury in the protein crystallography area organized by beamline instrument are to be found at http://dlwebres.dl.ac.uk/dl_public/publications/index.jsp). The examples below cite extreme cases of the large unit cell (virus and multi-macromolecular) cases, weak anomalous-scattering signal in MAD, fast time-resolved Laue

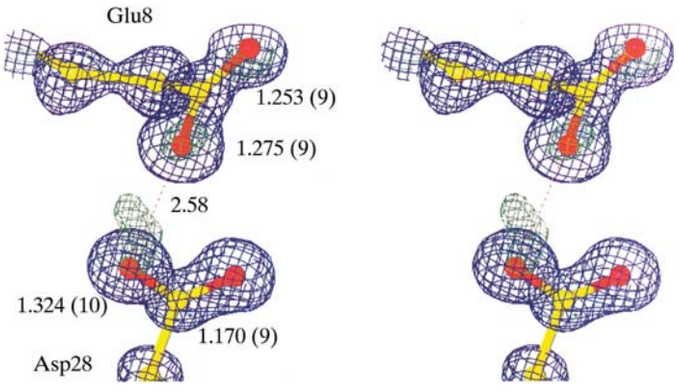

Figure 8.1.8.1
Determination of the protonation states of carboxylic acid side chains in proteins *via* hydrogen atoms and resolved single and double bond lengths. After Deacon *et al.* (1997) using CHESS. Reproduced by permission of The Royal Society of Chemistry.

studies and the ultra-high-resolution and even valence-density structure determinations to date. Another phasing technique involving multiple ('*n*-beam') diffraction is also being applied to proteins [Weckert & Hümmer (1997) at the ESRF and the NSLS]. These examples at least indicate the present bounds of capability of the various sub-fields of SR and macromolecular crystallography.

8.1.8.1. Atomic and ultra-high-resolution macromolecular crystallography

The use of high SR intensity, cryo-freezing of a protein crystal to largely overcome radiation damage and sensitive, automatic area detectors (CCDs and/or image plates) is allowing diffraction data to be recorded at resolutions equivalent to smaller-molecule (chemical) crystallography. In a growing number of protein crystal structure studies, atomic resolution (1.2 Å or better) is achievable (Dauter *et al.*, 1997). The 'X-ray data to parameter' ratio can be favourable enough for single and double bonds, *e.g.* in carboxyl side chains, to be resolved [Fig. 8.1.8.1; Deacon *et al.* (1997) for concanavalin A at 0.94 Å resolution]. Along with this bond-distance precision, one can see the reactive proton directly. This approach complements H/D exchange neutron diffraction studies. Neutron studies have expanded in scope by employing Laue geometry in a synergistic development with SR Laue diffraction (Helliwell & Wilkinson, 1994; Helliwell, 1997*b*; Habash *et al.*, 1997, 2000); a comprehensive survey of neutron macromolecular crystallography, instruments and results in determining the atomic details of protonation and hydration has been given by Blakeley (2009). In particularly well ordered protein structure cases, valence-electron-density descriptions are possible for those atoms with *B* factors ~<3 $Å^2$ [see *e.g.* Guillot *et al.* (2008) and Luger (2007)]. The scope and accuracy of protein crystal structures has been transformed. A diffraction-component precision index for characterizing the overall precision of protein structures has been given by Cruickshank (1999) and cast in terms of experimental parameters by Blow (2002).

8.1.8.2. Small crystals

Compensating for small crystal sample volume by increasing the intensity at the sample has been of major interest from the outset, and tests showed that the use of ~20 μm-sized samples is feasible (Hedman *et al.*, 1985). Third-generation high spectral brightness sources were optimized for this application *via* micron-sized focal spot beams, as described in the *ESRF Foundation Phase Report* (1987). Applications of the ESRF microfocus beamline diffractometer (Perrakis *et al.*, 1999) include as an example the determination of the structure of the bacteriorhodopsin crystal at high resolution from micro-crystals (Pebay-Peyroula *et al.*, 1997). Experiments using extremely thin plates involving only 1000 protein molecular layers are described by Mayans & Wilmanns (1999) on the BW7B wiggler beamline at DESY, Hamburg. A variety of small crystals and SR, including tabulated sample scattering efficiencies, can be found in Helliwell (1992), pp. 410–414 and more recently in Riekel *et al.* (2005). The ESRF Upgrade (Fig 8.1.2.2) will push this into the sub-micron territory.

8.1.8.3. Time-resolved macromolecular crystallography

Time-resolved SR Laue diffraction of light-sensitive proteins, such as CO Mb studied with sub-nanosecond time resolution in pump–probe experiments (see Srajer *et al.*, 1996), have shown direct structural changes as a function of time. Enzymes, likewise, are being studied directly by time-resolved methods *via* a variety of reaction initiation methods, including pH jump, substrate diffusion and light flash of caged compounds pre-equilibrated in the crystal. Flash freezing is increasingly used to trap molecular structures at optimal times in a reaction determined either by microspectrophotometry or repeated Laue 'flash photography'. Enzyme reaction rates can be altered through site-directed mutagenesis (*e.g.* see Niemann *et al.*, 1994; Helliwell *et al.*, 1998) and matched to diffraction-data acquisition times. For overviews, see the books edited by Cruickshank *et al.* (1992) and Helliwell & Rentzepis (1997), the recent review by Bourgeois & Weik (2009) and the companion chapter by Moffat (Chapter 8.2 in this volume).

8.1.8.4. Multi-macromolecular complexes

There is now a wealth of results in this field and the reader must be referred to books such as Liljas *et al.* (2009) for a detailed exposition. Multi-macromolecular complexes, such as viruses (Rossmann *et al.*, 1985; Acharya *et al.*, 1989; Liddington *et al.*, 1991) (Fig. 8.1.8.2), the nucleosome (Luger *et al.*, 1997), light-harvesting complex (McDermott *et al.*, 1995) and the 13-subunit membrane-bound protein cytochrome *c* oxidase (Tsukihara *et al.*, 1996), and large-scale molecular assemblies like muscle (Holmes, 1998) are very firmly recognizable as biological entities whose crystal structure determinations relied on SR. These single-crystal structure determinations involved extremely large unit cells and became tractable despite very weak scattering strength. The crystals often showed extreme sensitivity to radiation (hundreds, even a thousand, crystals have been used to constitute a single data set). Cryocrystallography radiation protection is now used extensively in crystallographic data collection and was critical for work with ribosome crystals (Hope *et al.*, 1989); SR has been essential for these structure determinations (see *e.g.* Yonath, 1992; Yonath *et al.*, 1998; Ban *et al.*, 1998; Wimberley *et al.*, 2000; Noller, 2005). A very large multi-protein complex solved using data from the Daresbury SRS wiggler is the F_1 ATPase structure (Fig. 8.1.8.3), for which a share in the Nobel Prize for Chemistry in 1997 was awarded to John Walker in Cambridge. The structure (Abrahams *et al.*, 1994; Abrahams & Leslie, 1996) and the amino-acid sequence data, along with fluorescence microscopy, show how biochemical energy is harnessed to drive the proton pump across biological membranes, thus corroborating hypotheses about this process made over many years. This

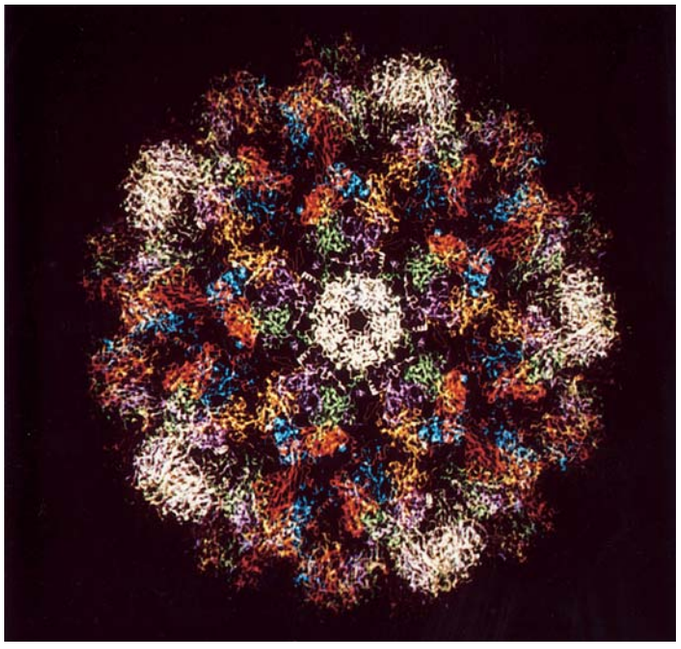

Figure 8.1.8.2
A view of SV40 virus (based on Liddington *et al.*, 1991) determined using data recorded at the SRS wiggler station 9.6 (Fig. 8.1.4.1*a*).

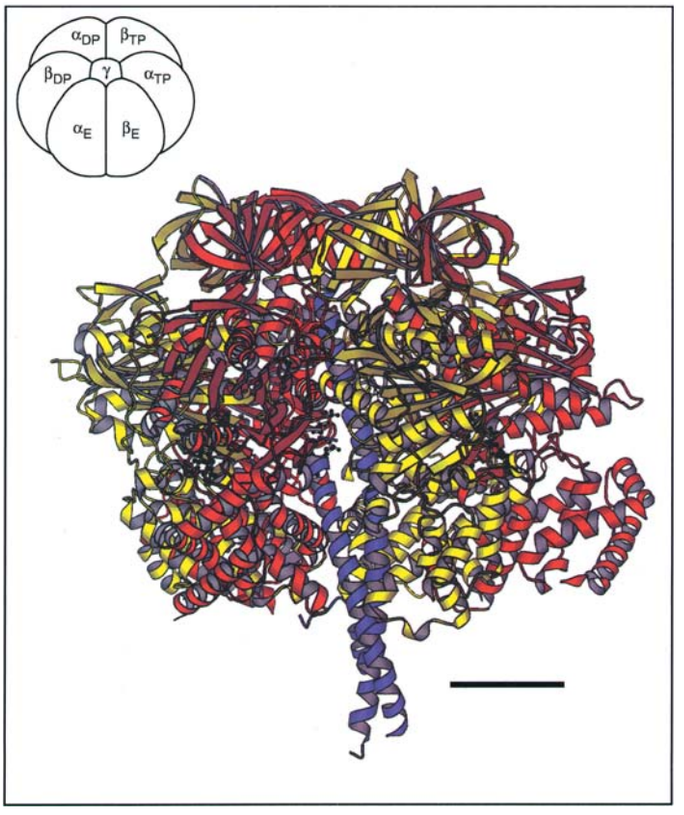

Figure 8.1.8.3
The protein crystal structure of F_1 ATPase, one of the largest non-symmetrical protein structure complexes, solved using SR data recorded on an image plate at the SRS wiggler 9.6, Daresbury. The scale bar is 20 Å long. Reprinted with permission from *Nature* (Abrahams *et al.*, 1994). Copyright (1994) MacMillan Magazines Limited.

study, made tractable by the SRS wiggler high-intensity protein crystallography station (Fig. 8.1.4.1), illustrates the considerable further scope that became possible with third-generation SR sources, such as the 780 Å diameter blue tongue virus (Grimes *et al.*, 1997, 1998) and the nucleosome core particle (Luger *et al.*, 1997). Spectacular progress has been made in the structural biology of photosynthesis using SR sources, which is not only yielding answers on this vital natural process but also stimulating much research to help address artificial energy sources based on this natural system. This research could have profound climate-change impacts with 'greener energy sources'. One such structure is the Photosystem II (PSII; see Fig. 8.1.8.4). This topic has been reviewed recently by Barber (2009); the atomic details of the Mn_4Ca cluster of PSII have proved to be especially challenging to X-ray study (Yano *et al.*, 2005). These large-scale molecular assemblies often combine electron-microscope and diffraction techniques with SR X-ray crystallography and diffraction for low-to-high resolution detail, respectively.

8.1.8.5. Optimized anomalous dispersion (MAD), improved multiple isomorphous replacement (MIR) data and 'structural genomics'

Rapid protein structure determination *via* the MAD method, notably involving seleno protein variants (Hendrickson *et al.*, 1990) as well as xenon pressure derivatives (see *e.g.* Schiltz *et al.*, 1997; Cianci *et al.*, 2001), and improved heavy-atom isomorphous replacement data are removing a major bottleneck in protein crystallography: that of phase determination. Databases of successful heavy-atom compounds (see *e.g.* Sugahara *et al.*, 2009) have been compiled and are increasingly sophisticated. Overall, as the number of protein structures in the Protein Data Bank doubles every few years, the possibility of considering whole genome-level structure determinations arises (Chayen *et al.*, 1996; Chayen & Helliwell, 1998). The human genome comprises some 35 000 genes. Of these, some 40% are coding for membrane-bound proteins, which are more difficult to crystallize. Since a MAD protein crystal structure currently requires less than 1 day of SR BM beamtime, the new 'bottlenecks' are protein production and crystallization. Thus, structural genomics projects have established 'pipelines' for protein structure determination with a view to creating a complete 'protein folds space'. This approach, along with homology modelling and genetic alignment techniques, opens the immense potential for structural genomics to yield huge numbers of experimentally derived protein structures and thereby a much better basis for understanding and controlling disease through structure-based drug design and

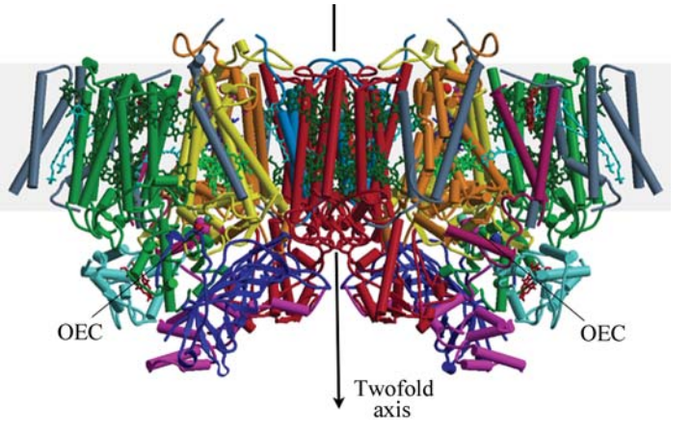

Figure 8.1.8.4
Side view of the structure of Photosystem II, the water-splitting enzyme of photosynthesis, determined using X-ray crystallography based on data recorded at the SLS and ESRF (Ferreira *et al.*, 2004). Kindly provided by Professor So Iwata, Imperial College, London.

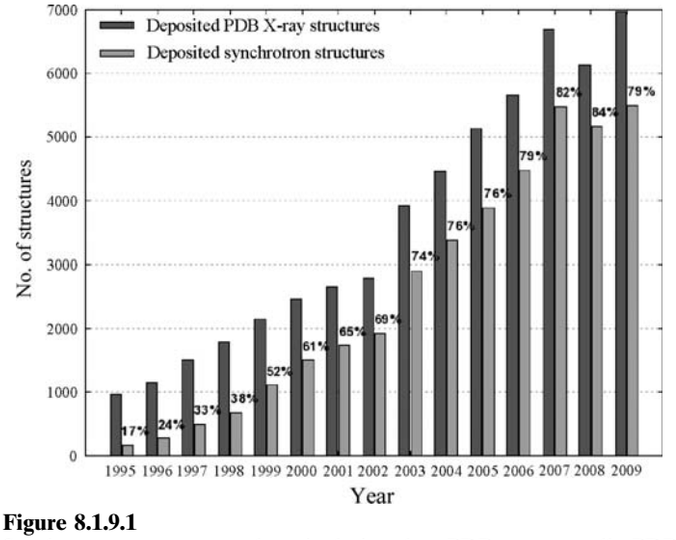

Figure 8.1.9.1
Synchrotron structures deposited in the PDB *versus* all PDB deposited structures (from http://biosync.rcsb.org/BiosyncStat.html) as of December 2009, *i.e.* a majority of all determined macromolecular crystal structures are now synchrotron-radiation derived.

discovery [for an early description see Bugg *et al.* (1993), for an example of pharmaceutical company collaboration see the Industrial Macromolecular Crystallography Association (IMCA) Collaborative Access Team at APS in Chicago (http://www.imca.aps.anl.gov/) and for a recent European perspective see *e.g.* Maclean *et al.* (2006).]

8.1.8.6. Radiation damage

The successes of these sources in macromolecular crystallography have been spectacular, so much so that provision of such beamlines now accounts for ~40% of the APS and ESRF insertion-device sectors. Nevertheless, X-radiation damage has been a continuing concern not least as the 'cutting edge' of capability to study ever-smaller crystals and ever-larger unit cells at synchrotron-radiation sources has been improved and optimized. A notable development has been a series of International Workshops on X-ray Damage to Crystalline Biological Samples. Most of these workshops have resulted in special issues of the *Journal of Synchrotron Radiation* (Volume 9 part 6, Volume 12 part 3, Volume 14 part 1 and Volume 16 part 2). The latest of these has a mini-review by Garman & Nave (2009).

8.1.9. Concluding remarks

SR and crystallography are now intricately intertwined in their scientific futures and in facilities provision (see *e.g.* Helliwell, 1998; Dauter, 2006; Fig. 8.1.9.1). Jiang & Sweet (2004) have given a systematic analysis of the impact of SR on macromolecular crystallography capabilities.

The new XFELs have produced very novel possibilities for 3D structure determination not only of non-crystallizable proteins but also whole cells (Neutze *et al.*, 2000; Miao *et al.*, 2001; Sayre, 2008; Shapiro, 2008). Whilst these approaches have attracted controversy, they represent a bold new push of X-ray diffraction methods towards widening capabilities in important frontiers in structural biology and structural cellular biology.

References

Abrahams, J. P. & Leslie, A. G. W. (1996). *Methods used in the structure determination of bovine mitochondrial F_1 ATPase. Acta Cryst.* D**52**, 30–42.

Abrahams, J. P., Leslie, A. G. W., Lutter, R. & Walker, J. E. (1994). *Structure at 2.8 Å resolution of F1-ATPase from bovine heart mitochondria. Nature (London)*, **370**, 621–628.

Acharya, R., Fry, E., Stuart, D., Fox, G., Rowlands, D. & Brown, F. (1989). *The 3-dimensional structure of foot and mouth disease virus at 2.9 Å resolution. Nature (London)*, **337**, 709–716.

Allinson, N. M. (1994). *Development of non-intensified charge-coupled device area X-ray detectors. J. Synchrotron Rad.* **1**, 54–62.

Amemiya, Y. (1997). *X-ray storage phosphor imaging plate detectors: high sensitivity X-ray area detector. Methods Enzymol.* **276**, 233–243.

Andrews, S. J., Hails, J. E., Harding, M. M. & Cruickshank, D. W. J. (1987). *The mosaic spread of very small crystals deduced from Laue diffraction patterns. Acta Cryst.* A**43**, 70–73.

Arndt, U. W., Greenhough, T. J., Helliwell, J. R., Howard, J. A. K., Rule, S. A. & Thompson, A. W. (1982). *Optimised anomalous dispersion crystallography: a synchrotron X-ray polychromatic simultaneous profile method. Nature (London)*, **298**, 835–838.

Arnold, E., Vriend, G., Luo, M., Griffith, J. P., Kamer, G., Erickson, J. W., Johnson, J. E. & Rossmann, M. G. (1987). *The structure determination of a common cold virus, human rhinovirus 14. Acta Cryst.* A**43**, 346–361.

Arzt, S., Campbell, J. W., Harding, M. M., Hao, Q. & Helliwell, J. R. (1999). *LSCALE – the new normalization, scaling and absorption correction program in the Daresbury Laue software suite. J. Appl. Cryst.* **32**, 554–562.

Baker, P. J., Farrants, G. W., Stillman, T. J., Britton, K. L., Helliwell, J. R. & Rice, D. W. (1990). *Isomorphous replacement with optimized anomalous scattering applied to protein crystallography. Acta Cryst.* A**46**, 721–725.

Ban, N., Freeborn, B., Nissen, P., Penczek, P., Grassucci, R. A., Sweet, R., Frank, J., Moore, P. B. & Steitz, T. A. (1998). *A 9 Å resolution X-ray crystallographic map of the large ribosomal subunit. Cell*, **93**, 1105–1115.

Barber, J. (2009). *Photosynthetic energy conversion: natural and artificial. Chem. Soc. Rev.* **38**, 185–196.

Bartunik, H. D., Clout, P. N. & Robrahn, B. (1981). *Rotation data collection for protein crystallography with time-variable incident intensity from synchrotron radiation sources. J. Appl. Cryst.* **14**, 134–136.

Beuville, E., Beche, J. F., Cork, C., Douence, V., Earnest, T., Millaud, J., Nygren, D., Padmore, H., Turko, B., Zizka, G., Datte, P. & Xuong, N. H. (1997). *A 16 × 16 pixel array detector for protein crystallography. Nucl. Instrum. Methods*, **395**, 429–434.

Bilderback, D. H. (1986). *The potential of cryogenic silicon and germanium X-ray monochromators for use with large synchrotron heat loads. Nucl. Instrum. Methods*, **246**, 434–436.

Blakeley, M. P. (2009). *Neutron macromolecular crystallography. Crystallogr. Rev.* **15**, 157–218.

Blewett, J. P. (1946). *Radiation losses in the induction electron accelerator. Phys. Rev.* **69**, 87–95.

Blow, D. M. (2002). *Rearrangement of Cruickshank's formulae for the diffraction-component precision index. Acta Cryst.* D**58**, 792–797.

Bonse, U., Materlik, G. & Schröder, W. (1976). *Perfect-crystal monochromators for synchrotron X-radiation. J. Appl. Cryst.* **9**, 223–230.

Bourenkov, G. P., Popov, A. N. & Bartunik, H. D. (1996). *A Bayesian approach to Laue diffraction analysis and its potential for time-resolved protein crystallography. Acta Cryst.* A**52**, 797–811.

Bourgeois, D. & Weik, M. (2009). *Kinetic protein crystallography: a tool to watch proteins in action. Crystallogr. Rev.* **15**, 87–118.

Brammer, R., Helliwell, J. R., Lamb, W., Liljas, A., Moore, P. R., Thompson, A. W. & Rathbone, K. (1988). *A new protein crystallography station on the SRS wiggler beamline for very rapid Laue and rapidly tunable monochromatic experiments: I. Design principles, ray tracing and heat calculations. Nucl. Instrum. Methods A*, **271**, 678–687.

Branden, C. I. (1994). *The new generation of synchrotron machines. Structure*, **2**, 5–6.

Brinkmann, R., Materlik, G., Rossbach, J., Schneider, J. R. & Wilk, B. H. (1997). *An X-ray FEL laboratory as part of a linear collider design. Nucl. Instrum. Methods*, **393**, No. 1–3, 86–92.

Broennimann, Ch., Eikenberry, E. F., Henrich, B., Horisberger, R., Huelsen, G., Pohl, E., Schmitt, B., Schulze-Briese, C., Suzuki, M., Tomizaki, T., Toyokawa, H. & Wagner, A. (2006). *The PILATUS 1M detector J. Synchrotron Rad.* **13**, 120–130.

Bugg, C. E., Carson, W. M. & Montgomery, J. A. (1993). *Drugs by design. Sci. Am.* **269**, 60–66.